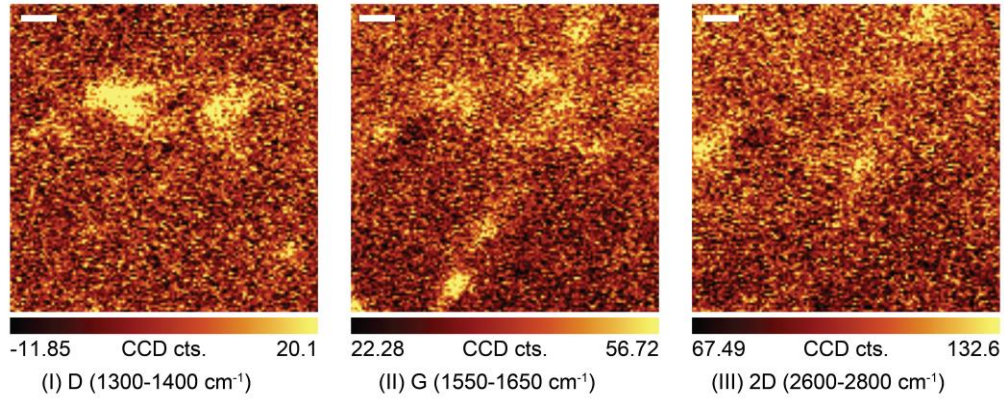


Supplementary Information

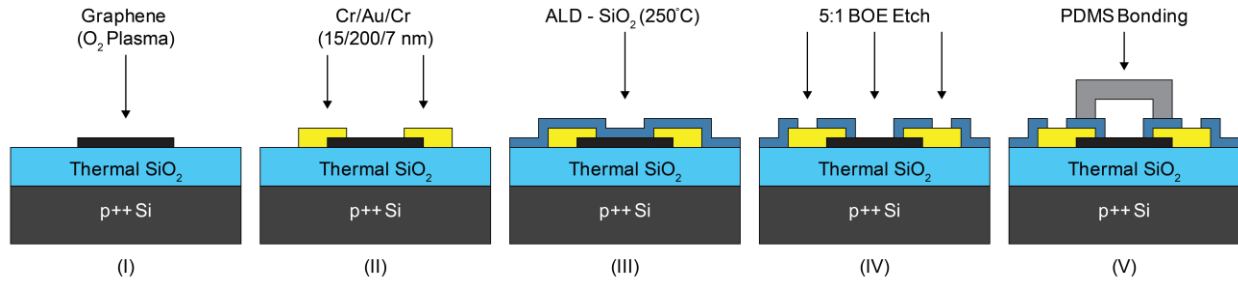
Supplementary Figure 1 | Raman spectroscopy of CVD graphene on SiO₂/Si substrate.



Integrated Raman intensity maps of D, G, 2D peaks, scanned across the same graphene area.

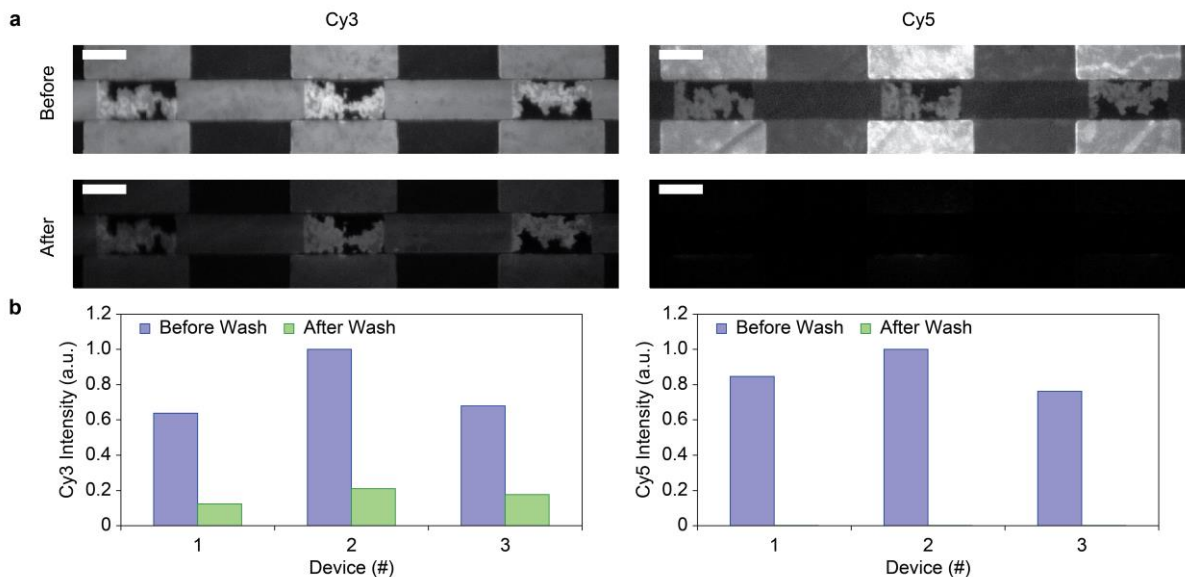
Scale bars: 1 μm . Our CVD-graphene is monolayer-dominated.

Supplementary Figure 2 | Additional fabrication details.



The use of Cr in the Cr/Au/Cr (15/200/7 nm) contacts to graphene is to facilitate adhesion to both the SiO₂ substrate below and the ALD-SiO₂ layer above. After BOE opening of these multi-stratified metallic contacts (step IV), the top Cr layer is removed with Cr-etchant 1020 to expose the Au layer, which makes a contact with bonding wire. PDMS is bound to the ALD-SiO₂ layer by a surface activation process of both the PDMS and the ALD-SiO₂ layer, which uses 120 mTorr 30-Watt O₂-plasma for 10 seconds (step V). To prevent graphene from being etched away in O₂ plasma, a small PDMS strip is put on the ALD-SiO₂ layer, fully covering the exposed graphene area but not directly touching the graphene.

Supplementary Figure 3 | Target DNA removal for control experiments of Fig. 2.

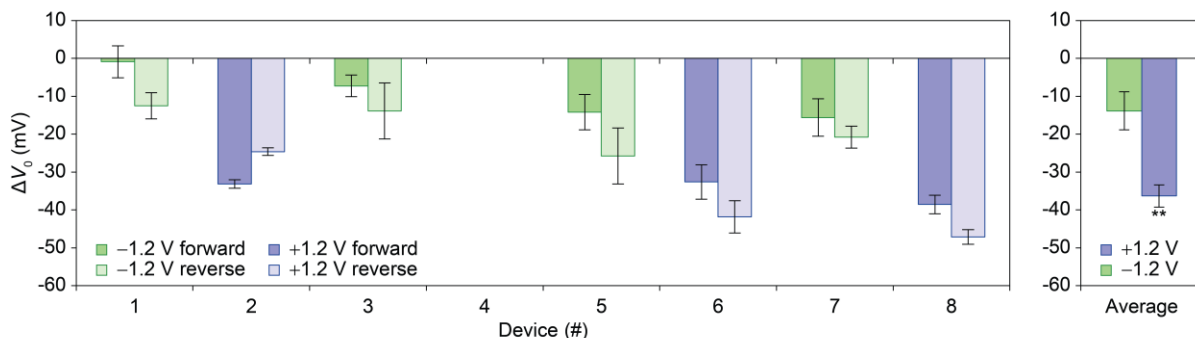


Scale bars: 50 μm . The control experiment of Fig. 2 of the main text is performed after target DNA hybridization experiment on the same graphene sensor array. To this end, we fully remove the hybridized target DNAs by 45-min 90°C de-ionized water wash. To verify the target DNA removal, another device array is functionalized with BSA and streptavidin, followed by a 10-minute passive immobilization of 200 nM probe DNA (labeled with Cy3) in 0.9 \times PBS and a 4-hour hybridization of 200 nM target DNA (labeled with Cy5) in 1 \times PBS. Subsequently, a 6 mL 0.005 \times PBS rinsing washes away non-hybridized target DNA. Confocal fluorescence images before the hot de-ionized water wash, shown in Supplementary Fig. 3a, confirm a significant amount of both immobilized probe DNA and hybridized target DNA on the graphene device array. But after the 45-min 90°C de-ionized water wash, the hybridized target DNA molecules are entirely removed while probe DNA molecules remain, as verified by another set of confocal fluorescence images, also shown in Supplementary Fig. 3a.

Fluorescence intensities, obtained from Supplementary Fig. 3a and shown in Supplementary Fig. 3b, reaffirm that the hot water wash leaves no discernible target DNA molecules. They also show that the wash not insignificantly removes probe DNA molecules themselves, leaving less than 30% of the originally immobilized DNA molecules. This is why we reintroduce BSA, streptavidin, and probe DNA for the control experiment of Fig. 2, which leads to comparable (or even increased) amount of probe DNA molecules for the 0.1 pM control experiments.

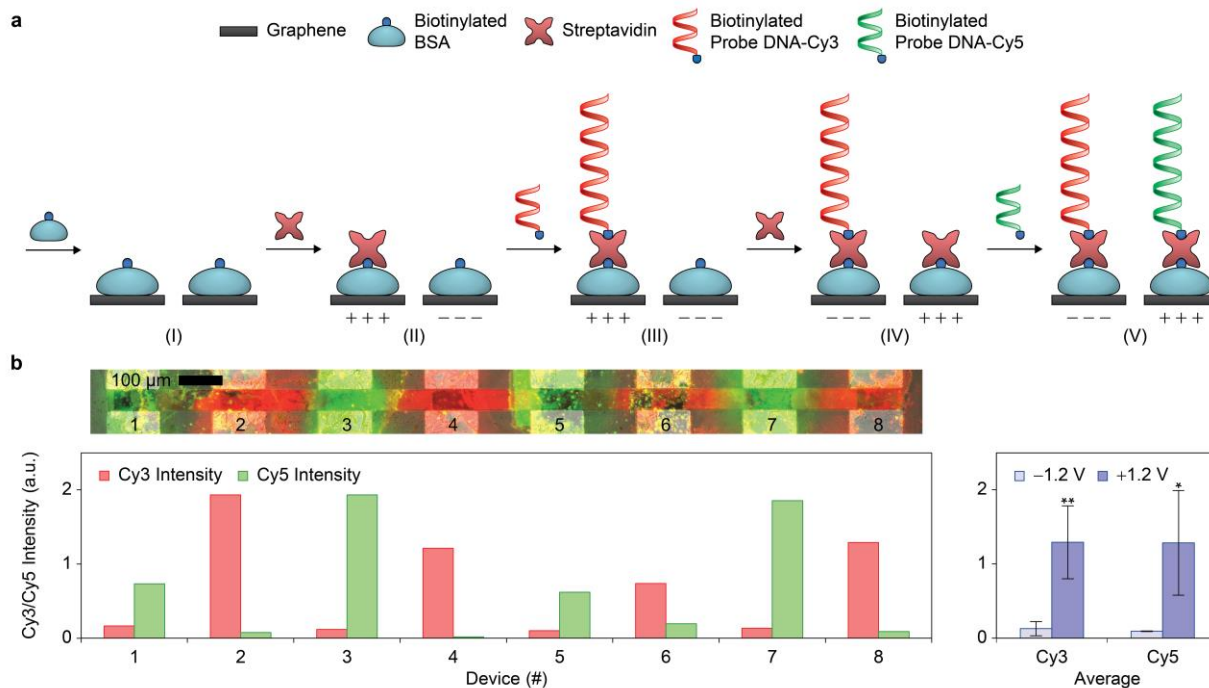
Supplementary Figure 4 | Repetition of the experiment of Fig. 3 by re-using the device of

Fig. 2.



The same type of experiment of Fig. 3, main text, was replicated with the graphene device array used for Fig. 2 after a further hot water wash (thus, this is the third use of the chip, following the target and control DNA hybridization experiments of Figure 2). The hybridization detection results are shown in Supplementary Fig. 4 above; the even-numbered graphene FETs show an average ΔV_0 of -36.2 ± 2.9 mV while the odd-numbered graphene FETs show a smaller averaged ΔV_0 value of -13.9 ± 5.0 mV. The larger V_0 shifts during this experiment for both even and odd numbered sites (and the appreciable shifts in the odd numbered sites where probe DNA is *not supposed* to be immobilized) as compared to those presented in Fig. 3 are attributed to extra immobilized probe DNA residue from the Fig. 2 experiments that were not completely washed (Supplementary Fig. 3). In addition, device 4 became open circuited due to the hot water wash. Nonetheless, the appreciable difference in ΔV_0 between the even- and odd-numbered sites clearly recapitulates the essence of the results of Fig. 3. For all data here: $*p < 0.05$; $**p < 0.01$; no *, not significant; and the error bars represent ± 1 s. d.

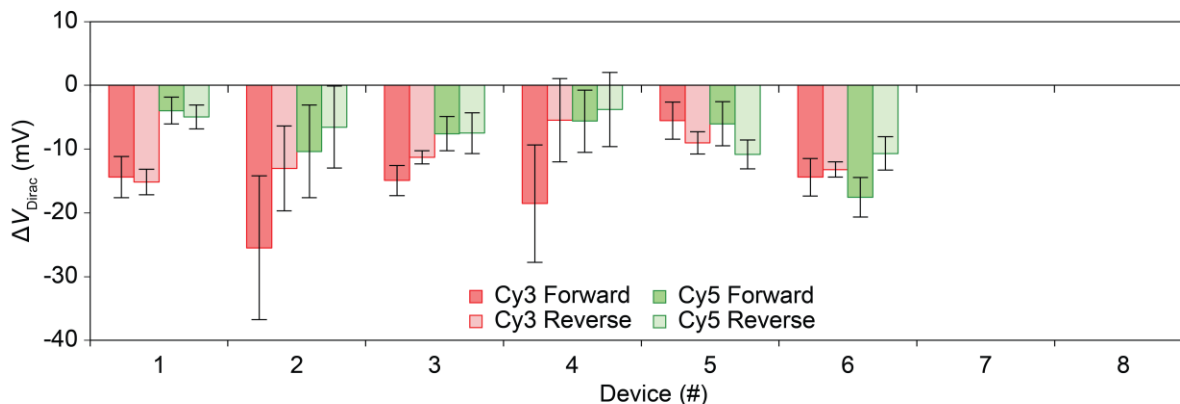
Supplementary Figure 5 | Similar repetition of the experiment of Fig. 5, by re-using the device used for Fig. 2 and Supplementary Fig. 4.



The experiment of Fig. 5 is similarly repeated with the graphene device array used for Fig. 2 and reused for Supplementary Fig. 4. For this re-reuse of the array, we wash it with 90°C de-ionized water for 45 minutes. The biasing scheme to immobilize Cy3-labeled probe DNA onto even-numbered sites is identical to Fig. 5. However, for immobilization of Cy5-labeled probe DNA, odd- [even-] numbered sites are biased at +1.2 V [-1.2 V], while in Fig. 5, the even-numbered sites are floated. A confocal fluorescence image (Supplementary Fig. 5b) clearly identifies Cy3-labeled probe DNA (red) and Cy5-labeled probe DNA (green) respectively in the even- and odd-numbered sites. Supplementary Fig. 5b, quantifies this clear pattern with the measured fluorescence intensity, with the Cy5 intensity normalized to the maximum Cy3 intensity. Correspondingly, in Supplementary Fig. 5b, the Cy3 intensity averaged across the 4 even-numbered sites is significantly higher than the Cy3 intensity averaged across the 4 odd-numbered

sites, and *vice versa* for the Cy5 intensity average (note that in Fig. 5b and Supplementary Figs. 3b and 5b, a direct quantitative comparison between Cy3 and Cy5 intensities is difficult, due to the calibration difference caused by the large background reflection from the substrate; however, this does not affect our analysis, because we focus on the amount of the same type of fluorophore across different sites). All these results re-attest to the electrophoresis-based site-selective immobilization. * $p < 0.05$; ** $p < 0.01$; no *, not significant; and the error bars represent ± 1 s. d.

Supplementary Figure 6 | Electrical measurements corresponding to Fig. 5.



After the site-selective immobilization of the two distinct sequences of DNA described with Fig. 5, we subsequently perform electrical detection of target DNA, now by using each graphene as a FET. Two distinct sequences of 10-pM target DNA, which are complementary to the Cy3- and Cy5-labeled probe DNAs, are used. Supplementary Fig. 6 shows ΔV_0 values measured after the hybridization phase. Device 7 is open circuited with no current through graphene—note, however, that this does not prevent the site-selective immobilization with device 7 (Fig. 5), as it can be still electrostatically biased with its drain and source voltages—and device 8 exhibits too noisy $V_{\text{REF}}-I_{\text{DS}}$ curves to meaningfully read ΔV_0 from. In devices 1 and 3, ΔV_0 after the hybridization phase with the target DNA complementary to Cy3 probe—let us call this Cy3 signal—is larger, while Cy5 signal is expected to be larger. Devices 2 and 4 show correct tendency with overall larger Cy3 signal, and device 5 shows somewhat correct tendency with overall slightly larger Cy5 signal as we compare forward and reverse sweep data separately. However, the separation between Cy3 and Cy5 signals is too insignificant in all these three devices (2, 4, and 5) to extract any useful correlation. Device 6 does not show any interpretable tendency. In sum, this electrical detection experiment fails to show any clear-cut meaningful

results, due likely to the reasons given in the main text, and calling for device improvement and electrophoresis optimization discussed in the main text. Error bars represent ± 1 s. d.

Supplementary Note 1 | Detailed account of Fig. 4a (transient electrolytic response).

To measure the transient electrophoretic time duration for the site-specific immobilization of Fig. 3 of the main text, we apply a voltage step between two adjacent graphene sites, and measure the resulting transient electrolytic current between the two sites (the transient currents were seen to be independent of the reference electrode biased at 0 V or floating). Fig. 4a shows the measured transient current for a voltage step of 1.0 V in 0.005× PBS. The transient current is characterized by a two-exponent decay, with the transient process terminated when charge redistribution across the graphene-electrolyte double layers is complete. Specifically, data fit reveal that the transient has time constants of 0.33 ms and 4.2 ms. The transient process is terminated in ca. 30 ms. The peak current is about 600 nA, and is measured to be linearly dependent upon the applied voltage step, which is also expected theoretically. From this, we estimate a peak current of $\sim 1.4 \mu\text{A}$ with a 2.4 V bias difference between two neighboring graphene sites.

Supplementary Note 2 | Detailed account of Fig. 4b (voltammogram).

To measure the DC current conducted through the graphene to the solution, a cyclic linear sweep is applied from the Ag/AgCl reference to graphene site in 0.005× PBS with the current measured, shown in Fig. 4b. The graphene site shown is from device 2 in an 8 graphene-device array with the remaining devices left floating. A scan rate of 10 mV/s is used; decreasing the scan rate shows little difference on the magnitude of the peak currents, suggesting that the majority of the current is attributed to Faradic processes instead of non-Faradic charging of the double layer capacitances. Based upon this, the DC steady state leakage current at both +1.2 V or -1.2 V is exponentially extrapolated to be between 1-10 nA to account for variances in the oxidation-reduction potentials amongst the devices.

Supplementary Note 3 | Calculation of transient and steady state charge transport.

The total transient charge transport caused by the application of biases during the site-specific immobilization in the experiment of Fig. 3 of the main text can be estimated by integrating the measured transient response current (Fig. 4a) and multiplying by a scalar to normalize to an applied voltage of 2.4 V. The resulting transient charge transport is 2 nC for 0.005× PBS, the PBS used in the experiment of Fig. 3. On the other hand, with the conservative estimate of 1 nA for the DC steady state graphene leakage current when biased at +1.2 V or -1.2 V (Fig. 4b), the total estimated DC steady state charge transport during 20 s is 20 nC. This suggests that the selective probe DNA deposition in our experiment of Fig. 3 with 0.005× PBS is dominated by the DC steady state leakage current rather than the transient current.

Supplementary Note 4 | Simulation of spatial pattern of the DC electric field magnitude.

As discussed in the main text and above, the DC steady state electrophoretic process contributes more charge transfer than the transient. With the applied symmetric potentials, weak but steady electric fields span across the even-numbered graphene sites and neighboring odd-numbered graphene sites to allow for DC graphene leakage current to flow. To get the feel for the spatial profile of this steady state electric field when positive [negative] biases are applied to the even- [odd-] numbered graphene sites, we perform a proof-of-concept simulation using COMSOL Multiphysics. A steady electric field in a resistive medium is an electrostatic field, therefore we can treat the electrolyte as a dielectric and estimate the electrostatic fields with our simplified simulation setup, which approximately mimics the steady state situation of the electrolyte.

Some details of the simulation setup are as follows. First, we arbitrarily set the dielectric constant of the electrolyte at 1, because we are primarily interested in the spatial field profile and will ultimately normalize the simulated electric field to the maximum. Second, we model the even- [odd-] numbered graphene sites as conducting electrodes at 1.2 V [-1.2 V], the reference electrode as a conducting electrode at 0 V, and metallic portions of the tubing as a floating electrode (the actual voltages across the solution are significantly smaller due to the voltage division caused by the large graphene double layer resistances and the far smaller electrolyte resistance). Third, in the setup, no DC current flows through the PDMS channel, plastic tubing, and SiO₂ substrate. Finally, small, yet non-zero, thickness is used for the conducting electrodes modeling graphene sites, in order to allow for a single mesh layer (~110 nm); a PDMS channel height of 60 μm, a graphene-to-graphene pitch of 240 μm, a graphene width of 90 μm, and a tubing width of 500 μm are used to replicate the actual system dimensions.

Figure 3c, top, of the main text shows the simulated electrolytic potential profile across the array and also across the height of the microfluidic channel. Figure 3c, bottom, of the main text displays the spatial pattern of the attractive electric field magnitude at the 110 nm height of the graphene conductor model, with a repulsive electric field for negatively charged molecules (*i.e.* an electric field direction pointing toward the substrate) magnitude set to zero. In Fig. 3c, bottom, a moving average of 20 μm has been also applied (*i.e.* the spatial profile is convoluted with a 20 μm square wave) to smooth the data and then normalization to the maximum has been performed. In the simulated result (Fig. 3c, bottom), the overall attractive field magnitude profile variation across different even-numbered graphene sites is due to the reference electrode, located in the outlet, and the metallic portions of the tubing.

Finally, note that the attractive electric field magnitude profile of Fig. 3c, bottom, recapitulates, in essence, the measured spatial distribution of the immobilized probe DNA (Fig. 3b). The detailed profile difference between simulation and measurements is well expected, because our simulation is rather simplified, and in the actual experiment, there are fluid flow effects (and associated downward/upward forces) as well as detailed electrochemical effects.